Journal of Power Sources 241 (2013) 159–167

Contents lists available at SciVerse ScienceDirect

Journal of Power Sources

journal homepage: www.elsevier.com/locate/jpowsour

$La_{0.7}Sr_{0.3}MnO_3$-coated SS444 alloy by dip-coating process for metallic interconnect supported Solid Oxide Fuel Cells

Leandro da Conceição [a,b], Laurent Dessemond [b], Elisabeth Djurado [b], Mariana M.V.M. Souza [a,*]

[a] Escola de Química – Universidade Federal do Rio de Janeiro (UFRJ), Centro de Tecnologia, Bloco E, sala 206, CEP 21941-909 Rio de Janeiro/RJ, Brazil
[b] LEPMI, Laboratoire d'Electrochimie et de Physico-Chimie des Matériaux et des Interfaces, UMR 5279, CNRS, Grenoble INP, Université de Savoie-Université Joseph Fourier, BP75, 38402 Saint Martin d'Hères, France

HIGHLIGHTS

- Single and double LSM layers were deposited by dip-coating on SS444 substrates.
- Chemical reactivity was detected at the interface of the substrate and LSM film.
- The oxidation resistance of the alloy is enhanced by one single LSM layer.
- ASR values as low as 0.6 mΩ cm^2 were recorded after 200 h at 800 °C.

ARTICLE INFO

Article history:
Received 26 February 2013
Received in revised form
8 April 2013
Accepted 11 April 2013
Available online 23 April 2013

Keywords:
$La_{0.7}Sr_{0.3}MnO_3$
Sol–gel
Area specific resistance
Metallic interconnect
SOFC

ABSTRACT

Sol–gel and dip-coating technologies have been used to deposit $La_{0.7}Sr_{0.3}MnO_3$ (LSM) porous thin films on stainless steel SS444-Cr-17% interconnect plates. Single and double LSM layers were fired in air at 800 °C for 2 h to achieve a sufficient adhesion on the substrate. The microstructure and composition of oxide scales were investigated using X-ray diffraction, scanning electron microscopy and energy dispersive X-ray analysis. The area specific resistance (ASR) for coated and uncoated plates was evaluated during long term oxidation in air at 800 °C for 200 h, and between 600 and 900 °C, by DC two point measurements. The formation of an interfacial oxide scale based on $(Cr,Mn)_3O_4$ spinel and Cr_2O_3 has been evidenced for uncoated and LSM-coated SS444. The results indicate that the oxidation resistance of the alloy is enhanced by a protective coating consisting of one single LSM layer. ASR values as low as 0.6 mΩ cm^2 were recorded after 200 h at 800 °C. The effectiveness of the LSM layer as a protective coating depends on the stability of the film and its adherence on the alloy substrate.

1. Introduction

Solid Oxide Fuel Cells (SOFC) have attracted a great attention as a new electric power generation system because of high energy conversion efficiency and an excellent long term stability during operation [1]. Ceramic materials are the basic components in SOFC. The high operating temperature of SOFC increases the electrode reaction rates but also enhances degradation of components and thus decreases the cell durability. The performance can be improved by a better control of the morphology of the different components and the reduction of the working temperature from 1000 °C to below 800 °C is likely to preserve the stability besides allowing the use of metallic interconnects instead of ceramic-based ones.

Many alloys based on iron, chromium and nickel have been investigated as interconnects for SOFCs [2–5]. Among these alloys, ferritic stainless steels are the alloy of choice for metal-supported SOFCs because they are quite inexpensive, have similar thermal expansion coefficients with other cell components, produce a thin, continuous and conductive chromia scale, and can have very long lifetimes at the SOFC operating temperature [6,7]. One of the major degradation problems when using these alloys is cathode poisoning by chromium from vaporization of the metallic interconnect. Several degradation mechanisms have been proposed in the literature [8–12]. In most of the proposed models, the oxidation of chromium oxide in the interconnect releases volatile Cr^{6+} species, such as CrO_3 and $CrO_2(OH)_2$, which are reduced at the triple phase boundary in the cathode leading to a rapid deterioration of the cell performance.

* Corresponding author. Tel.: +55 21 25627598; fax: +55 21 25627596.
E-mail address: mmattos@eq.ufrj.br (M.M.V.M. Souza).

0378-7753/$ – see front matter © 2013 Elsevier B.V. All rights reserved.
http://dx.doi.org/10.1016/j.jpowsour.2013.04.082

Several coating systems have been proposed for stainless steel interconnects to reduce chromium volatilization while maintaining low electrical resistance [13,14]. These coatings consist mainly of perovskite layers based on lanthanum strontium manganite or cobaltite, and manganese containing spinels, which are chemically and thermally compatible with other cell components [15–19]. A LSM dense layer may have greater efficiency in blocking chromium diffusion [15,20–23], but several works in the literature report that even a LSM porous film also shows excellent performance as barrier for the chromium diffusion [24–26].

The methods used for coating metallic interconnects have been reviewed recently [19] and include chemical vapour deposition, pulsed laser deposition, plasma spraying, screen printing, slurry coating, radio frequency magnetron sputtering, electrodeposition and sol–gel process. Among these methods, the sol–gel process provides several advantages: the microstructure and composition of the deposit can be easily controlled, deposition can be performed at low temperatures and the adhesion on the substrate is strong [27]. Despite these advantages, sol–gel method is not largely used for perovskite coating on metallic interconnects. Zhu et al. [28] used a sol–gel method to deposit lanthanum chromite on SS444, improving the oxidation resistance and scale adhesion on the alloy substrate after cyclic oxidation in air at 800 °C.

Cathodes based on lanthanum strontium manganite (LSM) are commonly used in SOFC, because of its high electrocatalytic activity for the O_2 reduction and a good chemical compatibility with electrolyte material based on zirconia. LSM-based materials have been investigated as protective coatings for chromia-forming metallic interconnects in oxidizing atmosphere [15,29–32]. Most of the reports indicate that LSM coatings change the oxidation behaviour of the base alloys and enhance the long term stability of metallic interconnects [20,21,33–35]. The area specific resistance (ASR) determined for a $(La_{0.80}Sr_{0.15})_{0.9}MnO_3$ layer slurry-coated on a Fe–16Cr alloy remained stable around 0.074 Ω cm^2 for 2600 h in air at 750 °C [15]. For LSM plasma-sprayed on SS444 substrate, the ASR remained lower than 0.02 Ω cm^2 for 165 h in air at 800 °C [24]. After an oxidation of 8000 h at 800 °C in air, the ASR of $(La_{0.80}Sr_{0.20})_{0.98}MnO_3$-coated Crofer22APU substrate reached a value of 0.023 Ω cm^2 [22]. This value is close to those reported by Quadakkers group for uncoated Crofer22APU during oxidation in air at 800 °C [36]. Regardless of the temperature, the oxidation behaviour of metallic interconnects depends on the nature of interfacial oxides formed between LSM coating and the substrate [19,32].

The aim of this study is to investigate LSM films as direct protective coatings for metallic SOFC interconnect, using a simple deposition technique. For this purpose, $La_{0.7}Sr_{0.3}MnO_3$ (LSM) single and double layers were deposited by sol–gel/dip-coating on commercial ferritic stainless steel (SS444). SS444 is an alloy with high corrosion resistance for applications at high temperatures, due to its high chromium content (17–19%) and additives such as niobium (Nb) and molybdenum (Mo). Moreover, the SS444 alloy has lower difference in thermal expansion coefficient to the ceramic coating and higher thermal conductivity than austenitic steels, making it less susceptible to internal stress which may occur when subjected to temperature in corrosive media. The ASR of uncoated and LSM-coated SS444 was monitored during long-term oxidation (200 h) at high temperature (800 °C). The microstructure and composition of interfacial oxides were investigated using X-ray diffraction (XRD), scanning electron microscopy (SEM) and energy dispersive X-ray (EDX) analyses.

2. Experimental

Commercial ferritic stainless steel SS444 (ArcelorMittal, Brazil), containing 17.4 wt.% of chromium (Table 1), was used as substrate ($10 \times 10 \times 1$ mm^3). The surface of the substrates was sanded using SiC paper (400, 600, 1200 and 2400) and polished with diamond abrasives. The polished substrates were ultrasonically washed in several steps with deionized water, isopropyl alcohol and acetone during 10 min and then dried at 100 °C in a furnace.

LSM ($La_{0.7}Sr_{0.3}MnO_3$) precursors were synthesized using the sol–gel route. The solution of metal salts (concentration C_s) was prepared from $La(NO_3)_3 \cdot 6H_2O$ (99%), $Sr(NO_3)_2$ (99%), $Mn(NO_3)_3 \cdot 6H_2O$ (99%) (Vetec-Brazil), dissolved in distilled water in appropriate amounts. This solution was then added to an organic solution (concentration C_o) containing acetic acid, hexamethylenetetramine (HTMA) and acetylacetone to promote the polyesterification and polycondensation reactions [37]. The concentration of metal salts was 0.18 mol L^{-1} with $R = C_o/C_s = 3$. The solution was heated to 80 °C on a heating plate during approximately 1 h to reach the desired viscosity (50 mPa s). The as-obtained gel was then deposited on the substrate at room temperature by perpendicular dip-coating. Film deposition was carried out with a holding time of 40 s in the gel and a withdrawal speed of 50 mm min^{-1}. Subsequently, the samples were dried at 100 °C for 10 min, and thus a second layer could be possibly deposited. The coatings underwent a pre-heating treatment at 400 °C, and then were heated in air up to 800 °C at 2 °C min^{-1} for 2 h. Uncoated Fe–Cr alloy and alloys coated by one or two LSM layers will be referred to as SS444, SS444-1 and SS444-2, respectively.

The crystalline phases present were investigated by X-ray diffraction (XRD) using a PANalytical X'Pert Pro MPD diffractometer, with a 2θ speed of 2° min^{-1} from 10 to 90°. The crystallite sizes (D_{XRD}) and microstrain (ε) were calculated using the following equation [38]:

$$\beta\cos\theta/\lambda = 1/D_{XRD} + 4\varepsilon \sin\theta/\lambda \quad (1)$$

where θ is the diffraction angle, λ is the wavelength of incident radiation and β is the full width at half maximum (FWHM) of the peak. Plotting the $\beta\cos\theta/\lambda$ versus $4\sin\theta/\lambda$ a straight line yields the crystallite size from interception with the ordinate and microstrain from the slope.

Microstructures and elemental analysis of the deposited films were studied using scanning electron microscopy (SEM) with field-emission gun ZEISS Ultra 55 coupled with an energy dispersive X-ray (EDX) analyzer ZEISS 1540XB (Carl Zeiss NTS GmbH, Germany). For measuring the oxide scale thickness grown on the surface of the metallic substrate, cuts were made on the cross section of the uncoated and LSM-coated samples, then the samples were embedded in resin and subsequently cross-sectional surface was sanded with sandpaper 1200 and 2400 SiC and polished with diamond. The forming edges of the sample region (resin) were coated with a thin layer of platinum and the sample surface with a thin layer of carbon using a Sputter Coater, SCD brand, model 50.

Area specific resistance (ASR) of uncoated and LSM-coated alloys was measured as a function of time at 800 °C (isothermal

Table 1
Chemical composition of SS444 (in wt %) determined by X-ray fluorescence (XRF).

Fe	Cr	Mn	Si	Mo	Ti	Nb	C	Others
78.9	17.4	0.2	0.7	2.1	0.1	0.2	<0.1	N ≤ 0.030 (0.2 + 4(C + N) ≤ S + P ≤ 0.030 0.040)

heating for 200 h) and temperature between 600 and 900 °C (before and after isothermal oxidation) in air by using a DC two-point, four-wire probe approach [15]. The results related to the variation of ASR versus temperature have been recorded during a second thermal cycle upon heating. Indeed, some discrepancies have been evidenced for isothermal ASR values during the first cycle. Thus, at least the uncoated alloy can be regarded as pre-oxidized before ageing at 800 °C. Although pre-oxidation treatments are clearly effective in improving the corrosion resistance [2], the influence of isothermal ageing when coupled with LSM coating is likely to be similar [39]. In order to avoid any penetration of the metal electrode through the thin LSM coatings, platinum mesh (3600 mesh cm^{-2}) was used as current collector. As a consequence, Pt could be detected on the surface of the coating and in the cross-sectional morphology. To ensure an appropriate contact between the current collector and the investigated specimen, some constant load (100 g) was applied. A constant current from 1 to 10 mA imposed by a potentiostat/galvanostat (Radiometer PGS 201T) was passed through Pt probes and the voltage in the sample was measured using a multimeter (Hewlett–Packard 34401A).

During oxidation at high temperatures, the ASR of uncoated and LSM-coated alloys is affected by the resistivity of the interfacial oxide layer. By exposing alloys at high temperature, oxide scale is formed on both sides of the substrate. The ASR was calculated according to Ohm's law: ASR = $V/2i$, where V is the voltage drop and i the current density. The factor of 2 was added to take into account that the voltage drop was measured across two scales connected in series. The area was chosen equal to the geometric area covered by platinum meshes, according to the high conductivities of the substrate and LSM coating. By assuming that the resistivity of the alloy is negligible in comparison with that of oxide layers [2], ASR is directly related to both resistance and thickness of oxide scale and to the electrical properties of interface with the substrate. ASR measurements during oxidation at 800 °C in air were performed twice on uncoated and single layer coated alloys. The ASR values were observed to vary less than 10% in the chosen experimental conditions.

3. Results and discussion

3.1. Structural properties

Fig. 1 presents the X-ray diffraction patterns of SS444 (uncoated), SS444-1 (one LSM layer) and SS444-2 (two LSM layers) specimens, before and after isothermal oxidization at 800 °C for 200 h in air. Through XRD analysis of uncoated SS444, it is observed that the oxides formed on the alloy surface consist mainly of Cr_2O_3 and $(Cr,Mn)_3O_4$ with a spinel structure, in agreement with previous reports on Mn-containing Fe–Cr alloys [14,22,25]. The formation of $(Cr,Mn)_3O_4$ can be attributed to the high diffusion coefficient of manganese ions [25]. Moreover, the diffraction intensity of the Fe–Cr alloy significantly decreased after oxidation, which implies that the oxidation is basically controlled by the outward diffusion of cations from the alloy substrate, resulting in depletion of alloying elements and shrinking lattice parameters in the substrate near the oxide scale [40].

Within the experimental accuracy, only the LSM phase was detected for coated specimens after heating at 800 °C for 2 h (before oxidation) suggesting that no significant chemical reaction occurs between the perovskite phase and the Fe–Cr alloy. In agreement with literature data [22,25,31,32,34], Cr_2O_3 and $(Cr,Mn)_3O_4$ oxides were detected after the oxidation step, indicating that diffusion of chromium and manganese ions from the alloy occurs during the isothermal treatment at 800 °C in air.

The average crystallite sizes of the LSM coating were calculated according to Equation (1), before and after oxidation (Table 2). The

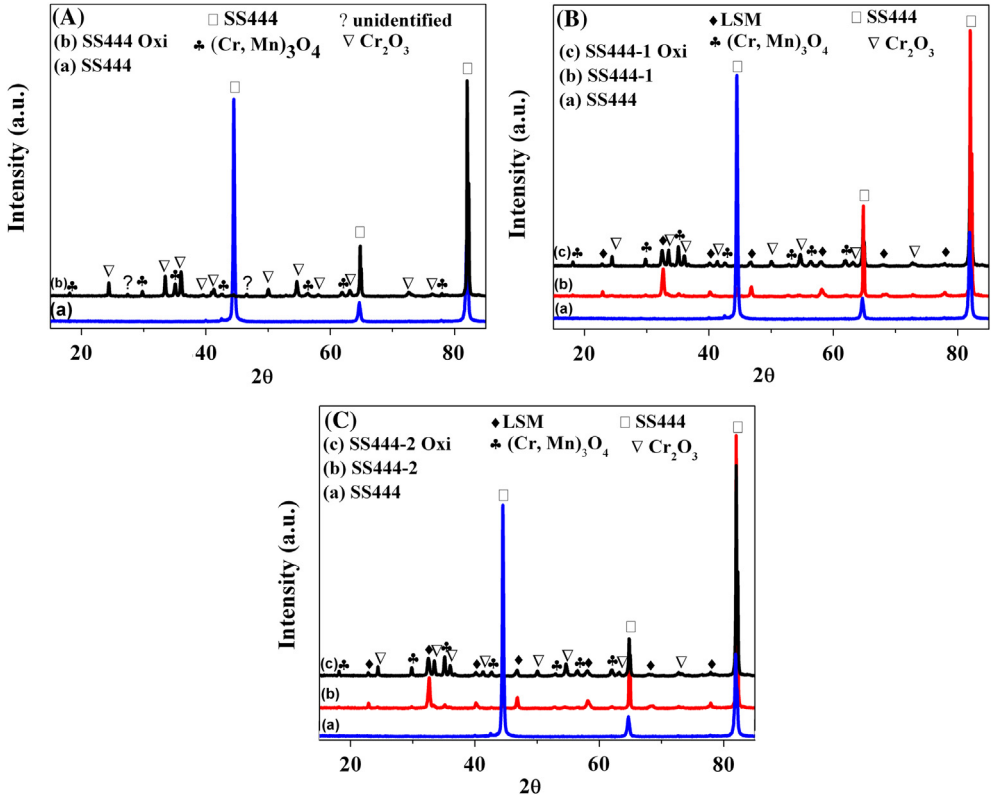

Fig. 1. XRD patterns of (A) SS444, (B) SS444-1 and (C) SS444-2 before and after (oxi) oxidation at 800 °C for 200 h in air. XRD pattern of SS444 before oxidation is reported in (B) and (C) for comparison.

crystallite size remains nearly constant after long term oxidation. Since the microstrain increases after oxidation, one can thus suggest that the crystal lattice distortion due to internal stresses becomes more severe upon heating. The SS444-1 and SS444-2 specimens are characterized by a similar average crystallite size, proving the high stability of the LSM film during the deposition process and during the oxidation treatment at high temperature. Orlovskaya et al. [41] calculated a crystallite size of $LaCrO_3$ thin film deposited on SS446 as 21.8 nm after annealing in air at 700 °C for 1 h.

3.2. Microstructural properties

As suggested by micrograph of the surface of uncoated alloy (Fig. 2a), the existence of residual pores corresponds to a partial spallation of the oxide scale. The thickness of the oxide scale is rather uniform and the average value is around 4 μm after 200 h at 800 °C in air (Fig. 3). Such a value agrees with literature data on uncoated alloys under similar experimental conditions. For instance, the average thickness of the oxide scale was measured at 3 μm for an uncoated Fe–Cr alloy containing 24% Cr and 1–5% Mn, after heating at 900 °C for 100 h in air [25]. The oxidation of Crofer22APU substrate at 800 °C for 100 h in air yields an oxide scale 10–11 μm thick [22]. For this same substrate, Stanislowski et al. [14] measured a thickness of 0.7–1.3 μm for the oxide scale after oxidation at 800 °C for 500 h in slightly humidified air.

From surface morphology of SS444-1 and SS444-2 (Fig. 2a and b), it is clear that the LSM coatings are porous, as expected when using dip-coating. The existence of necks between LSM particles indicates a partial sintering during the oxidation treatment. Furthermore, the presence of some faceted grains could be related to Cr_2O_3 and/or $(Cr,Mn)_3O_4$ phases [42]. Such grains can be observed because of the small coating thickness (Figs. 4 and 5). For the coating prepared with two LSM layers, some cracks are evidenced after oxidation (Fig. 2c). Since LSM is crystallized after thermal treatment for only 2 h at 800 °C (Fig. 1), these cracks are likely to originate from differences in thermal expansion coefficient (TEC) between the alloy and the LSM film [18,31,32], yielding the development of compressive residual stresses in the film during the cooling process [41]. Imperfect surface wetting of the second gel coating should also result in cracks already during drying at 100 °C. Such cracks were clearly evidenced for two LSM layers deposited on SS439 alloy [43]. The absence of any significant cracks for a single layer could be related to the more open microstructure of the coating. Indeed, some pores were observed on dense LSM film deposited by plasma sputtering on Fe–Cr alloys after oxidation at 800 °C for 200 h whereas no significant variation of the microstructure of screen printed LSM coatings on similar alloys was evidenced [32].

EDX analysis of uncoated alloy substrate (Fig. 3) indicates that the oxide scale (3) corresponds to chromium and manganese rich regions related to the growth of chromia and spinel phases, as evidenced by XRD (Fig. 1A). The strong peak related to carbon on the outer layer is associated with carbon deposition during preparation of the samples for EDX analysis (as described in Section 2). As could be expected, iron and chromium are the main elements in the bulk of investigated alloy (2). An enrichment of silica is evidenced at the alloy/oxide interface (4) and a higher content of Ti is detected in the oxide scale (3). In the absence of any LSM coating, one can thus deduce that manganese originates from the alloy and diffuses through the oxide layer [18]. For LSM-coated alloys, a more detailed EDX analysis has been performed (Figs. 4 and 5) to examine the diffusion across the coating/substrate interface. Indeed, LSM is expected to act as a barrier to oxygen when a coated specimen is exposed to high temperatures. This analysis was dedicated to determine the concentration distribution of various elements in the LSM/alloy interface. A schematic description of transport processes between a Fe–Cr alloy and a LSM coating is given in literature [13].

Table 2
Average crystallite size (D_{XRD}) of LSM phase and microstrain (ε) of LSM-coated SS444 before and after oxidation at 800 °C for 200 h in air.

Sample	Before oxidation		After oxidation	
	D_{XRD} (nm)	ε (%)	D_{XRD} (nm)	ε (%)
SS444-1	24.6	0.19	25.5	0.28
SS444-2	24.0	0.24	26.6	0.38

The first peculiar feature is that the thickness of the oxide scale is lower by using a LSM coating (1 μm against 4 μm for uncoated sample), in well agreement with literature data [25]. For instance, the average thickness of the oxide scale on Crofer22APU was around 25 μm after oxidation for 4000 h at 800 °C in air and it was only of the order of 8 μm after 7848 h by spray coating dense LSM on this alloy [22]. This last study agrees with the statements of Nie et al. [20] on the required morphology of the coating for an effective protection for corrosion. Nevertheless, a decrease of the oxide thickness after oxidation treatment has also been evidenced for porous LSM deposited by slurry-coating on SS430 alloy [15] and plasma spraying on SS444 substrate [24]. At this stage, it is worth noting that the growth rate of the oxide scale was reduced by using a thin and porous LSM film, and thus it can be regarded as an effective protection layer.

As indicated by XRD analysis (Fig. 1), the LSM phase is stable after oxidation at high temperature and a slight enrichment of chromium is detected in the interior of the coating layer (point 5 of Fig. 4). The segregation of Cr along the whole coating has already been reported for porous films on Fe–Cr alloys [22,25].

The elemental distribution of Cr (Figs. 4 and 5) indicates a higher concentration of chromium in the oxide scale (3) compared to the alloy/oxide interface (2), regardless of the specimen. This suggests that the growth of chromia is governed by diffusion of chromium ions through the oxide layer. These results are in agreement with previous reports pointing that the growth of chromia is a combination of apparent Cr^{+3} and O^{-2} diffusivities in Cr_2O_3 [23,44]. An outward diffusion of manganese is also likely and the Mn content is even higher in the vicinity of the LSM/oxide interface. An enrichment of oxygen is also evidenced. This was confirmed by additional analysis (6) performed at the alloy/oxide interface for SS444-1 and at the alloy/LSM interface for SS444-2. An inward diffusion of oxygen ions can be anticipated in the chosen experimental conditions, even with a LSM coating layer. Since the LSM coating layer could be regarded as an additional source of Mn, this element could, in principle, be transported by an inward diffusion to the coating/chromium oxide interface. Therefore, a further investigation of the Mn diffusion is required. The segregation of those elements suggests the formation of $(Cr,Mn)_3O_4$ at the outer surface of the oxide layer and Cr_2O_3 at the inner interface. An argument in favour of this statement is that manganese diffuses faster than chromium and is characterized by a low solubility in chromium oxide [32]. For both specimens, an outward diffusion of iron is also detected but its content becomes insignificant at the outer interface.

According to XRD analysis, no iron oxide was detected when a LSM coating is present, in agreement with thermodynamic predictions [45]. Thus, Cr- and (Cr,Mn)-based oxides can be regarded as oxide layers preventing the growth of Fe-based oxides [22]. Moreover, the formation of the spinel phase could reduce significantly the vaporization pressure of gaseous chromium species [25]. It is worth mentioning that the above statements agree with those presented by Quadakkers et al. [29] indicating that the transport of chromium is responsible for the formation of the spinel phase.

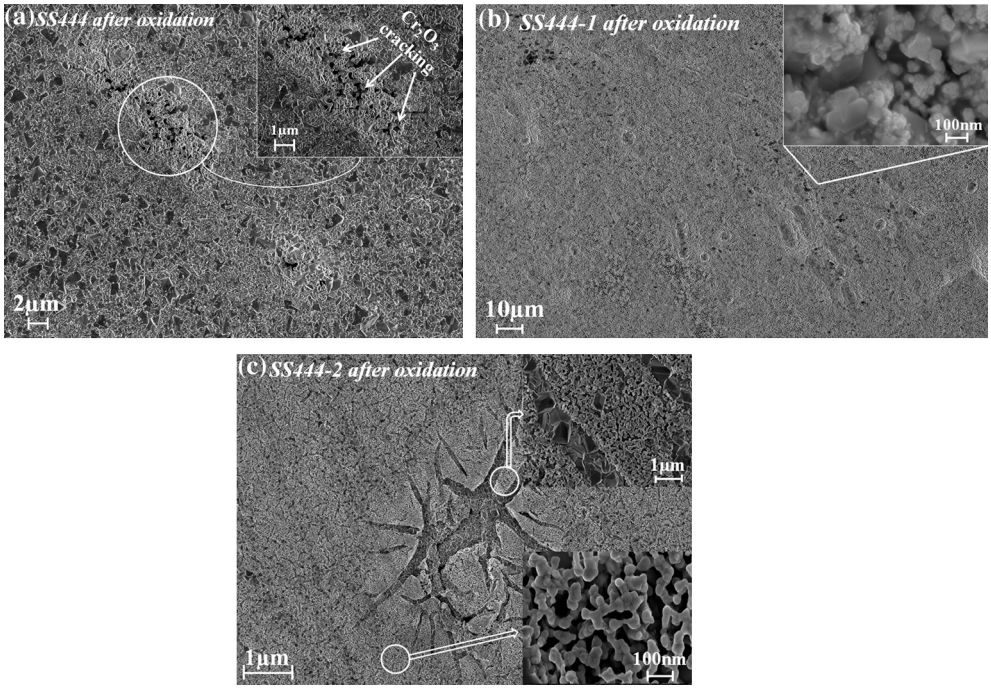

Fig. 2. SEM micrographs of the surface of (a) SS444, (b) SS444-1 and (c) SS444-2 after oxidation at 800 °C for 200 h in air.

Concerning the distribution of alloying elements, an enrichment of Ti was detected in the bulk of the alloy (7) and resulted in dark spheres. Accordingly, Ti diffusion from the alloy to the oxide scale can be predicted for coated specimens (Figs. 4 and 5), as suggested by Fergus [13]. At this stage, one can thus conclude that the well-faceted grains observed on the surface of SS444-1 after oxidation (Fig. 2b) are most likely due to the spinel phase, as already reported for Mn-containing Fe–Cr alloys [3,31]. For SS444-2 specimen, the

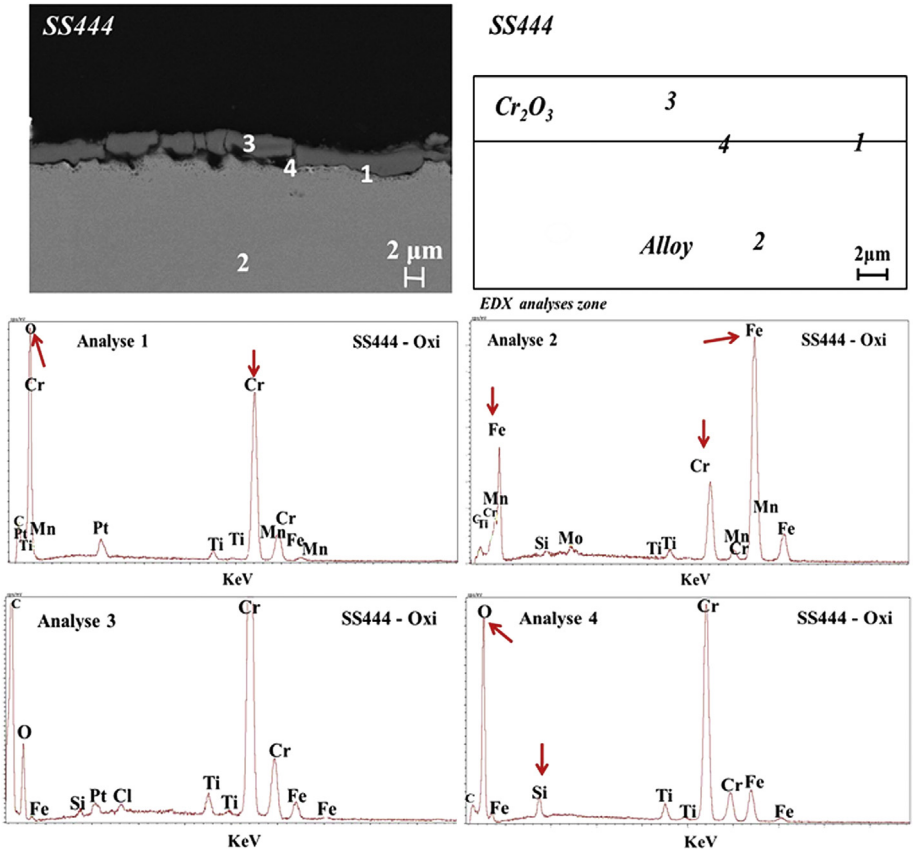

Fig. 3. SEM micrograph and EDX analyses of a polished cross-section of SS444 after oxidation at 800 °C for 200 h in air.

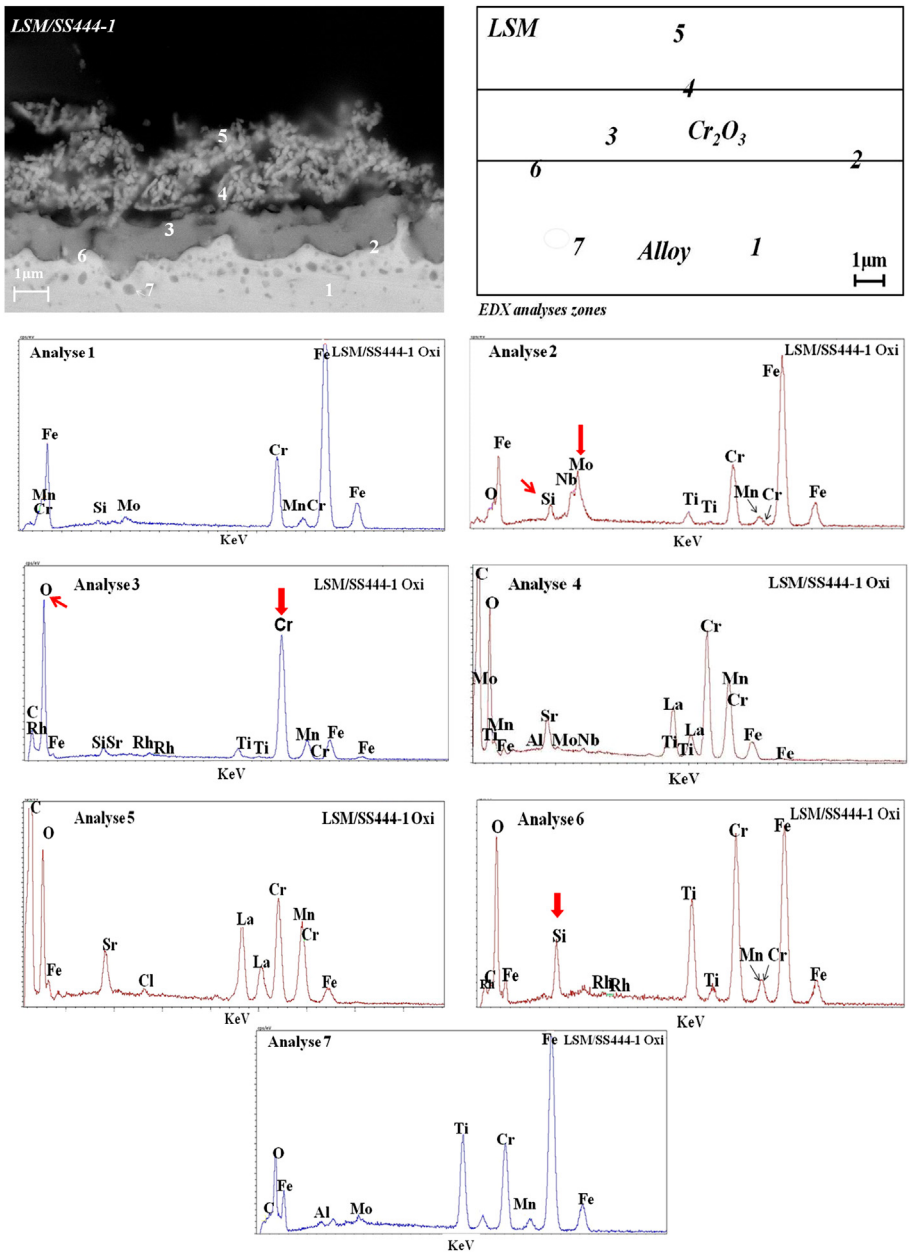

Fig. 4. SEM micrograph and EDX analyses of a polished cross-section of SS444-1 after oxidation at 800 °C for 200 h in air.

oxide scale thickness is less uniform in comparison with SS444-1, while is lower than that observed for uncoated alloy. This can be related to pit corrosion [46] due to gaseous oxygen diffusion through cracks in the LSM coating. This is consistent with a higher oxygen content at the oxide/LSM interface for two LSM layers (Fig. 6) and, thus, a higher flow of oxygen ions through the oxide scale can be anticipated.

3.3. Electrical properties

The variations of ASR for all investigated specimens versus oxidation time at 800 °C in air are given in Fig. 7. For uncoated alloy, the ASR dropped quickly from 30 mΩ cm^2 at the beginning of the test and then more slowly until a minimum of 15 mΩ cm^2 was reached after about 60 h. Thereafter, a sudden increase up to 45 mΩ cm^2 was observed followed by a slight decrease as a function of oxidation time until 200 h. An initial decrease of the ASR has also been reported in the literature for uncoated Fe–Cr alloys [47–49]. According to the literature, platinum could not be regarded as a complete inert material in contact with the oxide scale formed during long term oxidation [2,47,50], especially by using Pt paste. On the other side, no modification of the oxide layer morphology was detected when Pt covered the surface of a Fe–Cr alloy [51]. In this study, current collection was performed using platinum mesh and no significant variation of the oxide scale thickness was detected along the entire surface for oxidized SS444 specimens (Fig. 3). Accordingly, the observed ASR decrease can be related to an increasing contact area between platinum and the oxide scale, maybe due to a smooth scale surface and to the covering by the spinel phase, which is more conductive than chromia [18,25,32]. The sudden increase in ASR is likely to originate from partial spallation of the oxide layer [52] which causes a huge decrease of electrical contacts [48]. For an oxidation time greater than 60 h, one could expect that an intimate contact between platinum and the

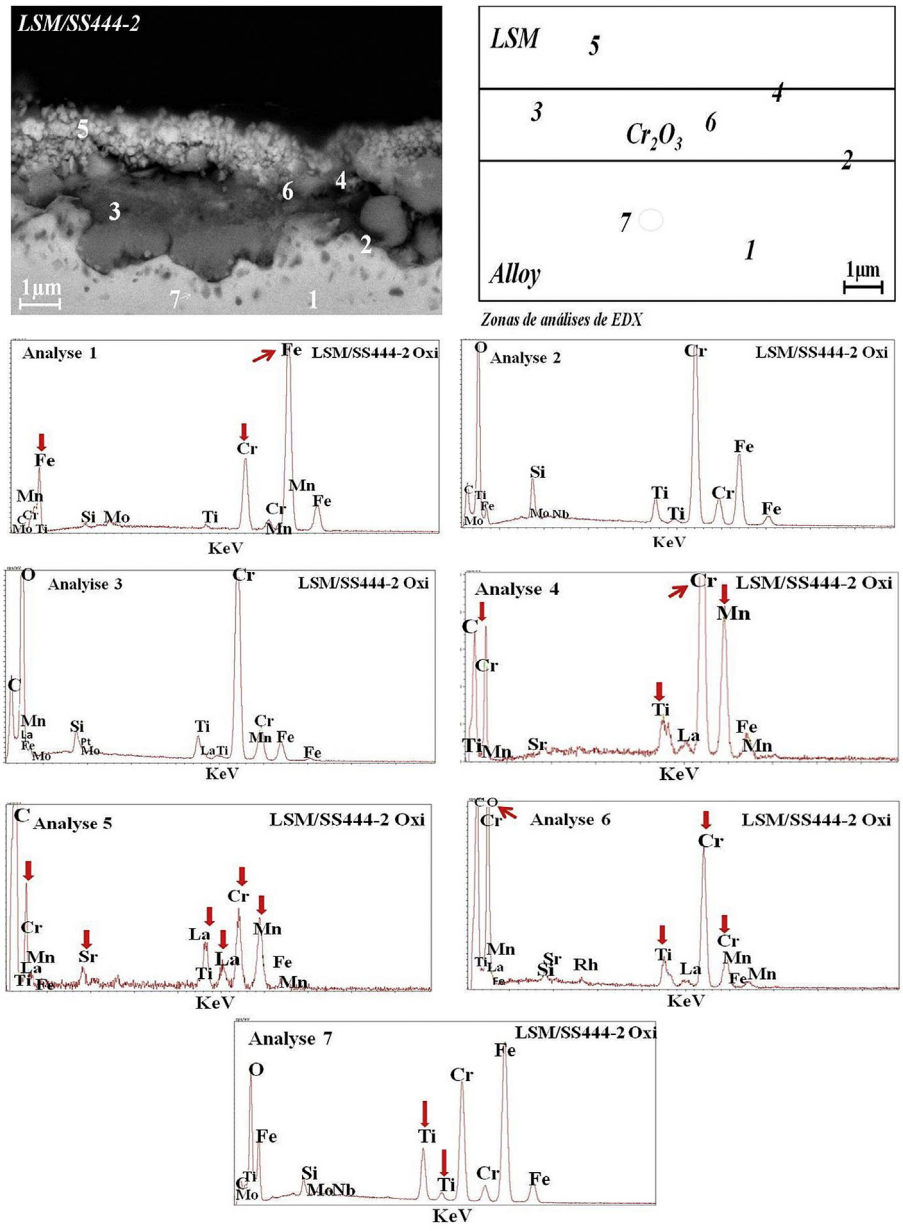

Fig. 5. SEM micrograph and EDX analyses of a polished cross-section of SS444-2 after oxidation at 800 °C for 200 h in air.

oxide scale should be favoured but the slower decrease of ASR with time (compared with the initial one) is due to another predominant contribution, i.e. the steady growth of chromia sublayer under the spinel phase [47]. The origin of the decrease after 180 h remains unclear but should not be due to any penetration of platinum into the oxide scale through the pores [2].

By coating SS444 alloy with one LSM layer, the initial ASR value (0.6 mΩ cm^2) is far lower than that recorded for uncoated specimen (Fig. 7). By assuming that an interfacial oxide layer grew during heating up to 900 °C (for ASR measurements versus temperature) and decreasing temperature down to 800 °C (for isothermal oxidation) [13], the observed difference can be related to increased contact area when using a porous LSM coating [18]. The higher the contact area, the lower is the contact resistance. As already observed for LSM-coated Fe–Cr alloys [21,34,35], the ASR of SS444-1 increases with time up to 1.3 mΩ cm^2 until 20 h. In the absence of any cracks in the LSM coating and any spallation of the oxide scale, the recorded increase is likely due to the continuing growth of the interfacial oxide of low conductivity [32]. After, the ASR steadily decreased down to 0.4 mΩ cm^2 until 140 h and remained constant till 200 h. A decrease of the ASR of coated alloys has been reported in the literature and was related to the crystallization of the LSM coating layer during isothermal oxidation in air [14]. According to the results of Fig. 1, this cannot be invoked; otherwise, the recorded decrease could be related to densification of the LSM layer and formation of the spinel phase, which is more conductive than chromia [33]. The nearly constant ASR value during oxidation at 800 °C in air suggests that the contact area between the LSM coating and the oxide scale remains nearly identical and that a semi-stable oxidation phase has been reached in the chosen experimental conditions. It is inferred from the above results that a single LSM thin film coated on SS444 can slow down the high temperature corrosion of this alloy. At this stage, it is worth mentioning that the final ASR value for SS444-1 is lower than a lot

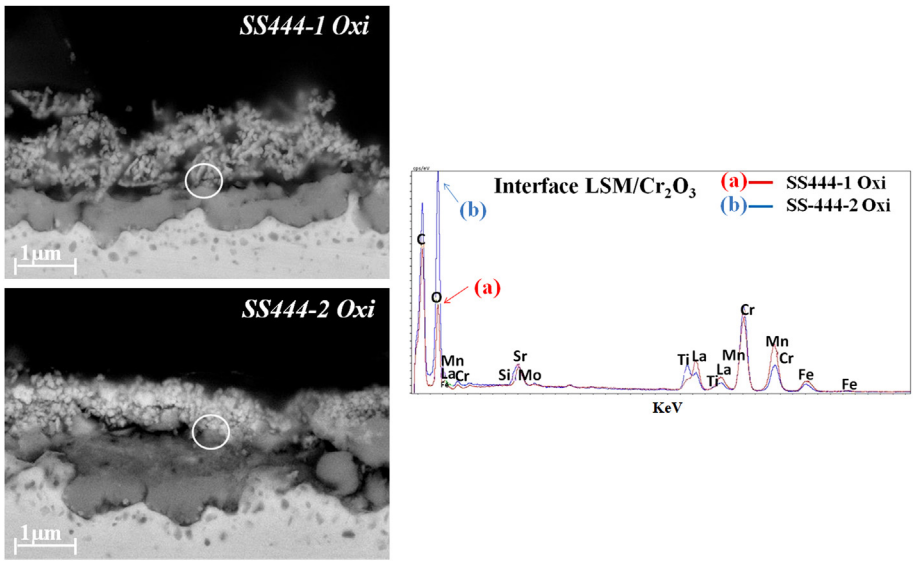

Fig. 6. EDX analysis at the oxide/coating interface for SS444-1 and SS444-2 after oxidation at 800 °C for 200 h in air.

of values reported in the literature [21,24,32,35,53,54]. Since an alloy must have an ASR below 100 mΩ cm^2 to be used as an interconnect in a practical SOFC [40,53], the observed ASR is encouraging at least for 200 h.

After depositing two successive LSM layers on SS444 alloy, the initial value of ASR is higher than by using one single LSM layer and is similar to that determined for uncoated alloy (Fig. 7). This is rather surprising if one refers to the high electronic conductivity of the LSM phase (about 100 S cm^{-1} at 800 °C in air) [55] and to the ASR behaviour of SS444-1. Moreover, the ASR of SS444-2 remains nearly constant until 40 h while that of uncoated alloy significantly decreases. Accordingly, the high ASR recorded could not be related to a poor bonding between the coating and platinum but rather between the LSM film and the alloy substrate. After 40 h of oxidation, the ASR of SS444-2 increases with time, indicating a low effectiveness of a two-layer LSM film in preventing the growth of the oxide scale. This can be related to the existence of cracks in the LSM layer as evidenced by SEM analysis (Fig. 2c).

To get additional information on the electrical properties of the investigated assemblies, the ASR was measured between 600 and 900 °C before and after the oxidation treatment since the oxide scale thickness is dependent on time and temperature [2,14]. Between 600 and 900 °C, the logarithm of (ASR/T) varies linearly versus the reciprocal temperature (1/*T*), regardless of the sample (Fig. 8). The corresponding activation energy (E_a) was calculated from the slope of the recorded linear curves and values are reported in Table 3. For oxidized SS444 and SS444-1, the activation energy is rather close to those determined by Hua et al. [40] (about 0.3 eV) for uncoated Fe–Cr alloy and by Kim et al. [15] (about 0.23 eV) for LSM coated SS430 alloy. One can also mention that these values are slightly lower than those obtained from the experimental data concerning oxide scales formed on different commercial stainless steel alloys reported by Montero et al. [49]. Since the activation energy for LSM is low in the chosen experimental conditions (0.10 eV) [56], the main contribution to the measured ASR is likely to be dominated by the oxide scale. It is worth noting that activation energy remains nearly unchanged and that the ASR only slightly increases after long term oxidation for SS444-1 sample, further confirming the good stability of one single LSM layer before and after oxidation and its effectiveness in reducing the alloy corrosion. In agreement with Hua et al. [40], the ASR of uncoated alloy is higher than that of SS444-1 at 900 °C, which can be related to a thicker oxide scale formed at high temperature.

For SS444-2 specimen, the situation is different. Indeed, the activation energy and the ASR value are lower before oxidation at high temperature (Table 3 and Fig. 8). By assuming that the electrical properties of the growing oxide upon heating and of the alloy/oxide interface are similar to those of the corresponding elements

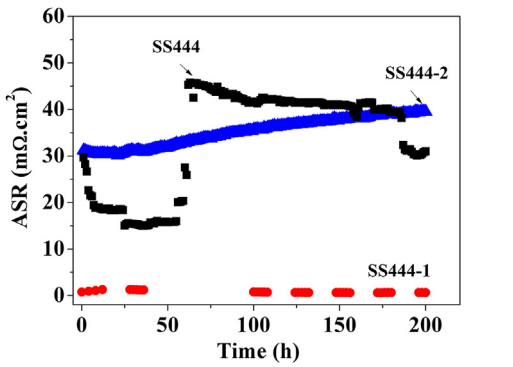

Fig. 7. Area specific resistance of uncoated and LSM-coated SS444 as a function of holding time at 800 °C in air.

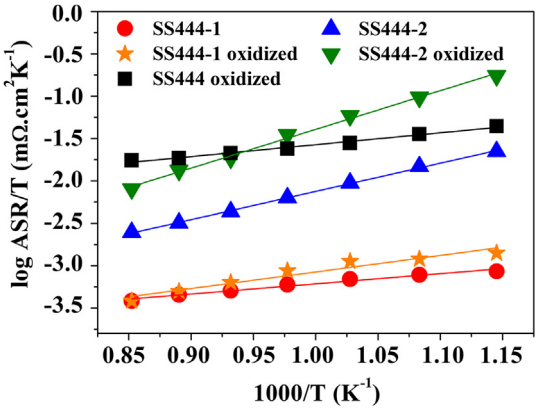

Fig. 8. Arrhenius diagram of ASR for uncoated and coated SS444 before and after oxidation at 800 °C for 200 h in air.

Table 3
Activation energy for electrical conduction of uncoated and LSM coated SS444 before and after oxidation for 200 h in air (600 °C ≤ T ≤ 900 °C).

Sample	E_a (eV) Before oxidation	E_a (eV) After oxidation
SS444	–	0.28
SS444-1	0.24	0.29
SS444-2	0.66	0.90

in SS444-1, the recorded difference could be related to the outer interface between LSM and the oxide scale. An activation energy about 0.7 eV was determined for a cobalt-coated Crofer22APU steel between 300 and 800 °C and was related to the protective layer and oxide scale [33]. A degradation of the outer interface would result in an increasing ASR during cooling, as experimentally observed. Moreover, the higher activation energy (0.90 eV) is in good agreement with the one reported by Chen et al. [18] (0.85 eV) in the same temperature range for Mn–Co spinel coated SS430. The recorded increase is likely to be related to an increasing contribution of the electron transfer at the LSM/oxide interface [2], which is not in contradiction with the ASR degradation during the isothermal dwell at 800 °C. The observed variation of ASR versus temperature further indicates that coating SS444 alloy by two LSM layers is not efficient to protect it from corrosion at high temperature.

4. Conclusions

Thin porous LSM coating layers were deposited successfully on a Fe–Cr alloy by dip-coating. The whole surface is fully recovered by LSM coating with good adhesion. The formation of an oxide scale between the substrate and the LSM film, consisting in $(Cr,Mn)_3O_4$ at the outer surface of the oxide layer and Cr_2O_3 at the inner interface, was evidenced during oxidation at 800 °C for 200 h in air. The thickness of the oxide scale was lower for LSM-coated alloys than for uncoated specimen indicating that LSM represents an efficient protective coating. The ASR was equal to 0.6 mΩ cm^2 for one LSM layer-coated SS444 after an exposure at 800 °C for 200 h in air. For the alloy coated by two LSM layers, a degradation of the outer interface was observed. It appears that one LSM layer coated on SS444 is effective for preventing growth of oxide scale in SOFC interconnect application but longer oxidation tests are required to warrant its use.

Acknowledgements

The authors thank CNPq – Brazil and Erasmus Mundus Programme (EBWII) for financial support granted to carry out this work. The authors also thank Rachel Martin and Stéphane Coindeau (C.M.T.C. – Consortium des Moyens Technologiques Communs – Institut Polytechnique de Grenoble – INP) for SEM and XRD analyses.

References

[1] S.C. Singhal, K. Kendall, Solid State Ionics 135 (2000) 305–313.
[2] K. Huang, P.Y. Hou, J.B. Goodenough, Solid State Ionics 129 (2000) 237–250.
[3] T. Brylewski, M. Nanko, T. Maruyama, K. Przybylski, Solid State Ionics 143 (2001) 131–150.
[4] K. Huang, P.Y. Hou, J.B. Goodenough, Mater. Res. Bull. 36 (2001) 81–95.
[5] Z. Yang, G.-G. Xia, J.W. Stevenson, J. Power Sources 160 (2006) 1104–1110.
[6] W.J. Quadakkers, J. Pirón-Abellán, V. Shemet, Mater. Res. 7 (2004) 203–208.
[7] M.C. Tucker, J. Power Sources 195 (2010) 4570–4582.
[8] J.W. Fergus, Int. J. Hydrogen Energy 32 (2007) 3664–3671.
[9] K. Hilpert, D. Das, M. Miller, D.H. Peck, R. Weiß, J. Electrochem. Soc. 143 (1996) 3642–3647.
[10] S.P. Jiang, J.P. Zhang, L. Apateanu, K. Foger, J. Electrochem. Soc. 147 (2000) 4013–4022.
[11] S.P. Jiang, S. Zhang, Y.D. Zhen, J. Mater. Res. 20 (2005) 747–758.
[12] H. Tu, U. Stimming, J. Power Sources 127 (2004) 284–293.
[13] J.W. Fergus, Scr. Mater. 65 (2011) 73–77.
[14] M. Stanislowski, J. Froitzheim, L. Niewolak, W.J. Quadakkers, K. Hilpert, T. Markus, L. Singheiser, J. Power Sources 164 (2007) 578–589.
[15] J.H. Kim, R.H. Song, S.H. Hyun, Solid State Ionics 174 (2004) 185–191.
[16] Z. Yang, G. Xia, S.P. Simner, J.W. Stevenson, J. Electrochem. Soc. 152 (2005) A1896–A1901.
[17] W. Qu, L. Jian, J.M. Hill, D.G. Ivey, J. Power Sources 153 (2006) 114–124.
[18] X. Chen, P.Y. Hou, C.P. Jacobson, S.J. Visco, L.C. De Jonghe, Solid State Ionics 176 (2005) 425–433.
[19] N. Shaigan, W. Qu, D.G. Ivey, W. Chen, J. Power Sources 195 (2010) 1529–1542.
[20] H.W. Nie, T.-L. Wen, H.Y. Tu, Mater. Res. Bull. 38 (2003) 1531–1536.
[21] S. Lee, C.-L. Chu, M.-J. Tsai, J. Lee, Appl. Surf. Sci. 256 (2010) 1817–1824.
[22] S.-S. Pyo, S.-B. Lee, T.-H. Lim, R.-H. Song, D.-R. Shin, S.-H. Hyun, Y.-S. Yao, Int. J. Hydrogen Energy 36 (2011) 1868–1881.
[23] M. Palcut, L. Mikkelsen, K. Neufeld, M. Chen, R. Knibbe, P.V. Hendriksen, Int. J. Hydrogen Energy 37 (2012) 14501–14510.
[24] D.P. Lim, D.S. Lim, J.S. Oh, L.W. Lyo, Surf. Coat. Technol. 200 (2005) 1248–1251.
[25] Y.D. Zhen, S.P. Jiang, S. Zhang, V. Tan, J. Eur. Ceram. Soc. 26 (2006) 3253–3264.
[26] H. Hwang, G.M. Choi, J. Electroceram. 22 (2009) 67–72.
[27] M. Gaudon, C. Laberty-Robert, F. Ansart, P. Stevens, A. Rousset, Solid State Sci. 4 (2002) 125–133.
[28] J.H. Zhu, Y. Zhang, A. Basu, Z.G. Lu, M. Paranthaman, D.F. Lee, E.A. Payzant, Surf. Coat. Technol. 177-178 (2004) 65–72.
[29] W.J. Quadakkers, H. Greiner, M. Hänsel, A. Pattanaik, A.S. Khanna, W. Mallener, Solid State Ionics 91 (1996) 55–67.
[30] J.Q. Li, P. Xiao, J. Eur. Ceram. Soc. 21 (2001) 659–668.
[31] E. Konysheva, J. Lautsch, E. Wessel, F. Tietz, N. Christiansen, L. Singheiser, K. Hilpert, Solid State Ionics 177 (2006) 923–930.
[32] C.-L. Chu, J. Lee, T.-H. Lee, Y.-N. Ching, Int. J. Hydrogen Energy 34 (2009) 422–434.
[33] Q.-X. Fu, D. Sebold, F. Tietz, H.-P. Buchkremer, Solid State Ionics 192 (2011) 376–382.
[34] C.-L. Chu, J.-Y. Wang, S. Lee, Int. J. Hydrogen Energy 33 (2008) 2536–2546.
[35] J.-J. Choi, J. Ryu, B.-D. Hahn, W.-H. Yoon, B.-K. Lee, J.-H. Choi, D.-S. Park, J. Alloys Compd. 492 (2010) 488–495.
[36] J. Froitzheim, G.H. Meier, L. Niewolak, P.J. Ennis, H. Hattendorf, L. Singheiser, W.J. Quadakkers, J. Power Sources 178 (2008) 163–173.
[37] P. Lenormand, S. Castillo, J.R. Gonzalez, C.L. Robert, F. Ansart, Solid State Sci. 7 (2005) 159–163.
[38] G.K. Williamson, W.H. Hall, Acta Metall. 1 (1953) 22–31.
[39] P. Yang, C.-K. Liu, J.-Y. Wu, W.-J. Shong, R.-Y. Lee, C.-C. Sung, J. Power Sources 213 (2012) 63–68.
[40] B. Hua, J. Pu, F. Lu, J. Zhang, B. Chi, L. Jian, J. Power Sources 195 (2010) 2782–2788.
[41] N. Orlovskaya, A. Coratolo, C. Johnson, R. Gemmen, J. Am. Ceram. Soc. 87 (2004) 1981–1987.
[42] M. Tsai, C.-L. Chu, S. Lee, J. Alloys Compd. 489 (2010) 576–581.
[43] L. Conceição, M.M.V.M. Souza, Thin Solid Films 534 (2013) 218–225.
[44] S.C. Tsai, A.M. Huntz, C. Dolin, Mater. Sci. Eng. A 212 (1996) 6–13.
[45] D.A. Jones, Atmospheric Corrosion and Elevated Temperature Oxidation, Macmillan Ed., 1992.
[46] T. Zhang, Y. Yang, Y. Shao, G. Meng, F. Wang, Electrochim. Acta 54 (2009) 3915–3922.
[47] Z. Yang, J.S. Hardy, M.S. Walker, G. Xia, S.P. Simner, J.W. Stevenson, J. Electrochem. Soc. 151 (2004) A1825–A1831.
[48] Z. Yang, G.-G. Xia, G.D. Maupin, J.W. Stevenson, Surf. Coat. Technol. 201 (2006) 4476–4483.
[49] X. Montero, F. Tietz, D. Stöver, M. Cassir, I. Villarreal, Corros. Sci. 51 (2009) 110–118.
[50] S.P. Simner, M.D. Anderson, L.R. Pederson, J.W. Stevenson, J. Electrochem. Soc. 152 (2005) A1851–A1859.
[51] G. Cabouro, G. Caboche, S. Chevalier, P. Piccardo, J. Power Sources 156 (2006) 39–44.
[52] H. Ebrahimifar, M. Zandrahimi, Solid State Ionics 183 (2011) 71–79.
[53] P. Piccardo, P. Gannon, S. Chevalier, M. Viviani, A. Barbucci, G. Caboche, R. Amendola, S. Fontana, Surf. Coat. Technol. 202 (2007) 1221–1225.
[54] F. Changjing, S. Kening, Z. Derui, J. Rare Earths 24 (2006) 320–326.
[55] J.X. Wang, Y.K. Tao, J. Shao, W.G. Wang, J. Power Sources 186 (2009) 344–348.
[56] J.W. Fergus, R. Hui, X. Li, D.P. Wilkinson, J. Zhang, Green Chemistry and Chemical Engineering Series, CRC Press, 2009, p. 179.